Quantum-Confined Nanostructures for Smart Optoelectronic and Theranostic Applications

Ratneshwar Kumar Ratnesh[1] and Abhinav Sharma[2]*

[1]Lincoln University College, Petaling Jaya, Selangor Darul Ehsan, 47301, Malaysia

[2]Institute of Post-LED Photonics, Tokushima University, 2-1 Minami-Josanjima, Tokushima, 770-8506, Japan

Email ID: ratnes123@gmail.com, pdf.ratneshwar@lincoln.edu.my, abhisharma.75@gmail.com

Abstract: Semiconductor quantum dots and their elongated zero-dimensional (0D) and one-dimensional (1D) counterparts are a major area of interest in solid state physics, materials chemistry and modern optoelectronic engineering. The electronic density of states (DOS) of these nanomaterials vary widely from continuous bulk bands to a structural and composition-dependent DOS and are 3D confined below the exciton Bohr radius. This review summarizes recent advances in both theoretical modelling of quantum confinement and synthetic paradigm of colloidal synthesis, hydrothermal synthesis, surface passivation by multi-shells and multidimensional structural heterostructuring (seeded nanorods). Importantly, we confront the use of alternative mirror boundary conditions in the context of the effective mass approximation to resolve discrepancies in the prediction of emission energies in the past. Lastly, the review contrasts the dual translation of these engineered architectures to next-generation optoelectronic circuitry (such as thin-film solar cell configurations, memristors, logic gates and deep-ultraviolet photodetectors) and multi-modal biomedical theranostics, which highlights remaining issues around heavy-metal toxicity, ligand-mediated charge transport barriers and physiological clearance kinetics.

Keywords: Bandgap Engineering, Quantum Confinement, Effective Mass Approximation, Seeded Nanorods, Core/Shell Heterostructures, Deep-Ultraviolet Photodetectors, Theranostics.

1. Introduction and Fundamental Physics of Quantum Confinement

In the early 1980s, the first observations by Brus, Efros and Ekimov of the deviations of the optical properties of nanocrystals from classical bulk semiconductor predictions changed the entire course of low-dimensional semiconductor physics [1]. As the physical size of an inorganic semiconductor crystal is scaled down to the sub-exciton Bohr radius of the material (RB), the movement of charge carriers created by the absorption of photons in the crystal is confined to a spatial region less than the usual bulk equilibrium distance of the electron and hole [2][3]. This is an extreme localization of the structure and this extreme localization results in the "quantum confinement effect", in which the continuous electronic energy bands found in bulk structures change into discrete energy levels that depend on the size of the structure, just like atomic and molecular energy levels [2][3]. This behavior is governed by the mathematical definition of the exciton Bohr radius, which relates it to the dielectric constant ε of the material, the mass of a free electron m0 and the reduced mass of the photogenerated exciton $\mu = (m_e \cdot m_h) / (m_e + m_h)$, with me and mh representing the effective masses of the electron and hole, respectively. This structural change will change the interaction of this material with incoming light fields.

The transformation from 1D to 2D leads to a dramatic modulation of the density of states (DOS) of the system, which is the number of available states of the orbitals in the volume V within an energy interval

dE between E and E + dE [3]. Bulk materials have a continuous DOS with a parabolic shape in three-dimensional space, but the length scale can be reduced through dimensions of nanoscale which limits the movement of the carriers along certain cartesian axes. If one axis is confined then a two-dimensional (2D) quantum well structure results with a step-like DOS distribution [3]. Restriction along two axes form a 1D quantum wire configuration. If all three dimensions are smaller than the Bohr radius of the exciton, then a zero-dimensional (0D) quantum dot is formed and the DOS is reduced to a very discrete delta function (δ) [3]. This collapse results in single-wavelength capacities of excitation and a dramatic focussing of oscillator strength into localized band-to-band transitions, which permit a sharp onset of the absorption spectrum and a very narrow, well-symmetric photoluminescence (PL) spectrum. This structural evolutionary cascade is just described in Figure 1.

At the same time, the energy gap between the valence band (VB) and conduction band (CB) is the fundamental optical bandgap (Eg) and varies inversely with the nanocrystal's physical radius. The fundamental property also enables continuous and seamless tuning of the light absorption and fluorescence emission from the dot, from the visible to the UV and the IR, just by varying the geometric boundaries of the dot. The larger quantum dots have a smaller quantum confinement effect, which means that the effective bandgap is reduced and the emission and absorption spectra exhibit a strong red shift, while the smaller particles exhibit strong quantum confinement effects which cause the effective bandgap to be increased and the emission and absorption spectra to shift towards a blue region. This operational flexibility overcomes the fixed-bandgap constraints of conventional planar semiconductors, removing lattice-mismatch barriers and laying the foundation for custom-tailored optoelectronic and biophotonic media. A dynamic optical range is available without modification of the basic chemistry, by scaling the physical dimensions below the exciton Bohr radius [1-3].

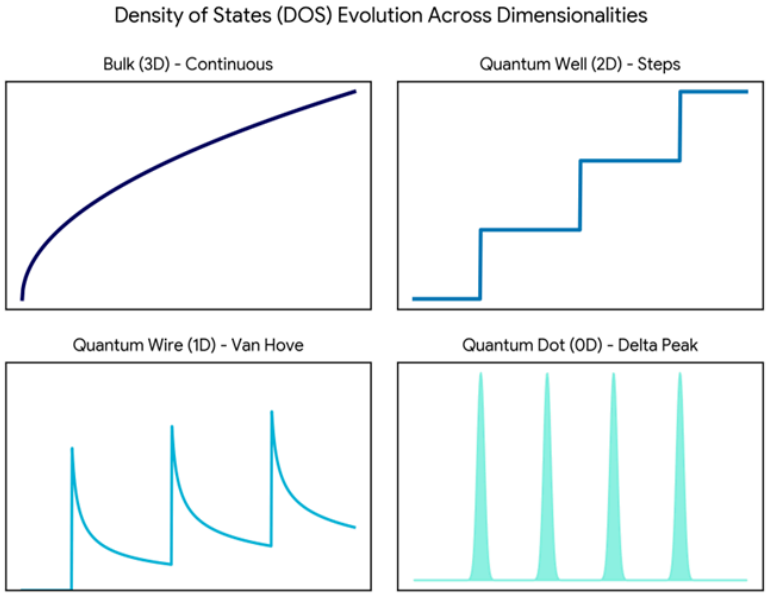

Figure 1: Mathematical evolution of the electronic density of states (DOS) cascading from continuous parabolic 3D bulk forms to discrete 0D delta function peaks.

2. Theoretical Bandgap Engineering: Resolving Boundary Models

Predictive Quantum mechanical models, by taking into account the effective mass approximation, are essential if the size tunable optical responses of quantum dots are to be fully exploited. In a spherical quantum dot of diameter ‘a’, traditionally, charge carriers are considered as particles confined in an infinite potential box of size a in three dimensions, with a potential energy V(r) equal to zero inside the sphere and to infinity at its physical boundary. These are “classical” or “impenetrable wall” boundary conditions, and the solution to the time-independent Schrödinger equation must be zero at the interface ($\Psi = 0$). This classical approach leads to a discrete energy spectrum given by $E = (h^2 / 8m\ a^2) \cdot (2n)^2$, with $n = 1, 2, 3...$ and thus the shift in the optical absorption threshold (ΔE) above the bulk bandgap is determined by $\Delta E = h^2 / (2\mu\ a^2)$. But a lot of data obtained from experiments showed that this model is not true to life [3].

The authors of this standard model have performed intensive experimental checks on highly spherical, monodisperse CdSe core and CdSe/ZnS core/shell quantum dots, and found that the standard model was much too high, sometimes by a factor of four, from the experimental values obtained through absorption spectroscopy. The mismatch is addressed in recent advanced models by the "even mirror boundary conditions," assuming specular reflection of an electron or a hole at the boundary of the nanocrystal. This physical change, similar to the wave phenomena seen in scanning tunneling microscopy (STM) experiments, has been observed in the vicinity of solid boundaries created by the interference of de Broglie waves reflected and incident upon the boundary. This weak confinement method allows for the matching of the values of the particle's wave function to the value of its virtual image away from the wall at an arbitrary point just inside the wall, so that the wave function does not vanish on the wall and partial quantum tunneling can occur into passivating mediums. This predictive energy alignment is verified graphically in Figure 2, with respect to the structural precision.

Application of this mirror-reflective framework reconstructs the radial eigen-function condition, yielding a modified energy spectrum: $E = (h^2 / 8m\ a^2) \cdot (2n + 1)^2$ for quantum states $n = 0, 1, 2...$ This mathematical restructuring alters the optical absorption threshold expression for the lowest ground-state exciton transition ($n = 0$), reducing it to $\hbar\omega = Eg + h^2 / (8\mu\ a^2)$. The statistical correlation of this mirror boundary paradigm with real-world spectroscopic data for CdSe ensembles of different diameters is outstanding, and it is able to capture confinement offsets that are out of reach for the impenetrable wall model, as reported in Table 1 for each of the sample points [2].

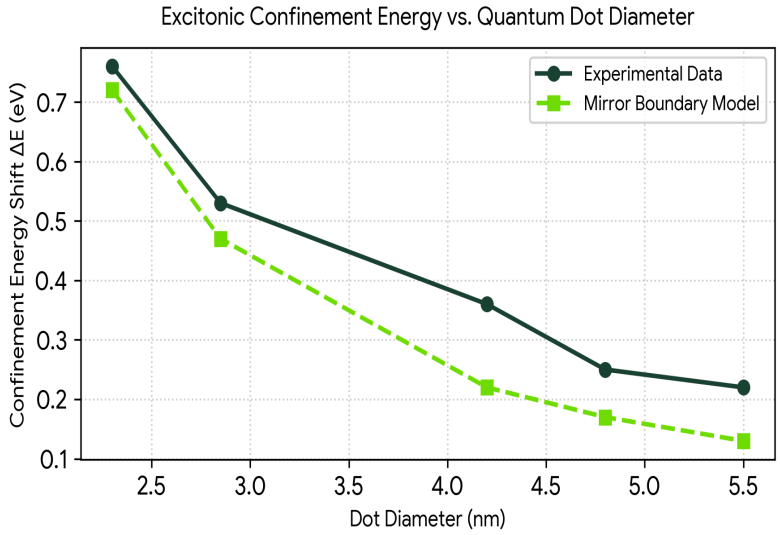

Figure 2: Statistical verification tracking empirical absorption thresholds against traditional impenetrable wall vs. mirror boundary models.

Table 1: Theoretical vs. Experimental Confinement Energy Values in Spherical CdSe Quantum Dots [2]

Dot Diameter (a, nm)	Experimental λ01 (nm)	Experimental Energy (eV)	Measured ΔE (eV)	Mirror Confinement (eV)
2.30	470	2.64	0.76	0.72
2.85	515	2.41	0.53	0.47
4.20	555	2.24	0.36	0.22
4.80	582	2.13	0.25	0.17
5.50	612	2.10	0.22	0.13

3. Advanced Synthetic Methodologies and Core/Shell Passivation Architecture

The synthesis of monodisperse, ordered and tunable band-gap quantum dots requires advanced colloidal, hydrothermal, and biomimetic chemistry. Isolation of highly monodisperse nanocrystals is still done mainly by the colloidal hot-injection synthesis protocol. This technique, developed in 1993 by Murray, Norris and Bawendi, was a bottom up approach and involved dissolving organometallic or metal-ion compounds within coordinating high boiling solvents under inert conditions. Rapid injection of cool precursor materials into a hot reaction mixture (usually around 300°C) results in the homogeneous induction of supersaturation, which in turn leads to an explosive and very short nucleation period; the precursor monomers are immediately consumed and the reaction temperature falls below the nucleation threshold. Further continuous heating leads to regular Ostwald ripening and the crystal dimensions are proportional to the reaction time. Conversely, room-temperature chemical synthesis has significant kinetic limitations, and comparative studies of the synthesis of CdSe over the years have shown that hot-injection methods consistently produce more uniform 2.5 nm dots with greater stability in their photoluminescence, whereas room-temperature synthesis is typically restricted to wider, more disordered 3.3 nm structures with higher defect densities [1][2].

The high cost, environmental risks and unpredictable safety characteristics of pyrophoric organometallic precursors such as dimethylcadmium (Me2Cd) have shifted the focus of industrial research towards safer, more environmentally friendly, and automated processes. The hydrothermal and aqueous-based configurations are designed to synthesize precursors at lower temperatures (~100°C to 220°C) with the

help of environmentally friendly stabilization agents like cysteamine or hydrazine hydrate to coordinate metal clusters in these configurations. Concurrently, biomimetic and mineralization techniques leverage natural biotemplates—including bovine serum albumin (BSA), lysozyme proteins, or localized microbial cultures—to mineralize ternary and binary dots (e.g., CuInS2 or ZnS) under ambient physiological conditions, ensuring that the embedded biological entities retain their functional target specificity. Additionally, machine learning pipelines are currently being used to control precursor flow rates and thermal zones dynamically in real time based on autonomous global search algorithms, which optimize photoluminescence quantum yields (PLQY) and reduce size distributions by using microfluidic reactors.

Regardless of the chosen synthesis pathway, unpassivated "core-only" quantum dots suffer from highly reactive surface configurations. Coordinating atoms situated at the physical boundary exhibit unsaturated, non-bonding electronic orbitals, commonly termed "dangling bonds". These dangling states introduce mid-gap trap levels within the dense density of states, acting as non-radiative recombination centers that quench fluorescence and lower the overall quantum yield to a meager 5% to 15%. This phenomenon and its structural mitigation are diagrammed schematically in Figure 3. To eliminate these surface traps, an epitaxial layer of a wider-bandgap inorganic semiconductor shell (such as ZnS, CdS, or ZnSe) is grown over the core domain. Passivating a CdSe core with a ZnS shell eliminates surface defects as visually abstracted in Figure 3(b), isolating the carrier wave functions within the core and raising the single-dot quantum yield past 90%. Growing specialized core-multishell networks provides structural protection that insulates the active core from moisture, heat, and photo-induced bleaching [3][4].

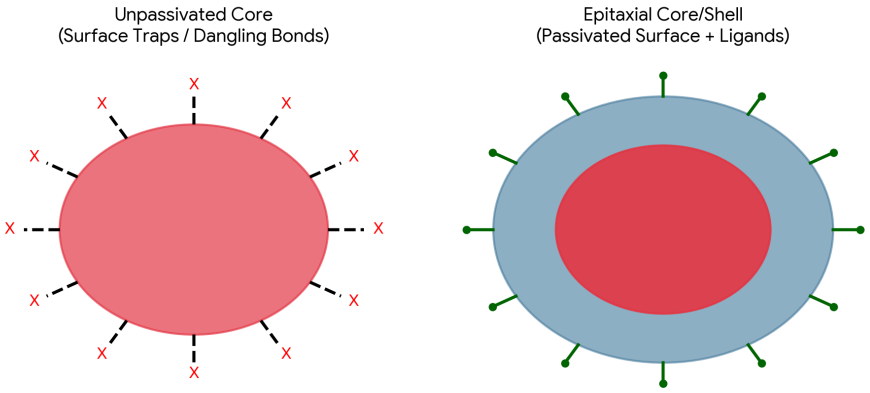

Figure 3: Schematic representation highlighting (a) an unpassivated core dominated by surface traps, and (b) an epitaxially covered core/shell layout wrapped with passivating ligand complexes.

4. Dimensional and Compositional Heterostructure: Seeded Nanorods

The relative electronic band alignment profiles of heterostructure nanorods are classified into three distinct categories, as shown in Figure 4 in the order that they will be discussed. For Type-I configurations, the entire bandgap of the core material is located and nested completely within the wider bandgap of the surrounding shell material, as illustrated in Figure 4(a). After light absorption occurs in this specific alignment, the excited electron and the hole both fall into the lowest possible electronic states, which are located inside the core seed, thereby increasing local radiative recombination.

In contrast, Type-II nanorods have a staggered band arrangement in which the conduction and valence band offsets force the spatial separation of the photogenerated charge carriers into different structural domains. When the electron becomes trapped in the conduction band of the flanking shell rod as illustrated in Figure 4(b), the hole will concurrently be pushed into the valence band of the core seed, giving rise to very long exciton lifetimes and characteristically large, red-shifted emissions.

Finally, a quasi-Type-II system corresponds to an intermediate case where either the valence or conduction band edges align very closely to each other. For CdSe/CdS seeded rods, the conduction band gap offset is small enough that the electron can freely delocalize and diffuse throughout the entire volume and length of the elongated nanorod shell, whereas the valence band offset ensures the hole remains strongly confined within the CdSe core seed, as shown in Figure 4(c).

Structural characterization methods have shown that the seed structure is not exactly centered in the geometric center of the rod-shell. Instead, it is located asymmetrically, about a third to a fourth of the total length from one tip. Selective metallic growth experiments were used as a visual check for this structural asymmetry. The addition of gold salts to a colloidal solution of seeded rods results in an electrochemical Ostwald ripening process that causes electrons to build up within the core seed. A localised charge concentration causes the reduction of the gold salts and the preferential growth of a unique metallic gold island immediately next to the embedded seed. The shape of the seeds determines the shape of the gold deposit, and the one-dimensional gold deposit obtained with the use of the one-dimensional rod-in-rod seeds illustrates how the external electronic interactions are determined by the seed morphology. The continuous rod-shells have a large physical volume, which makes them highly efficient photon-harvesting antennae with a multi-photon absorption cross-section up to 4 orders of magnitude larger than conventional 0D quantum dots [5].

Figure 4: Heterostructured Nanorod Electronic Alignment Regimes

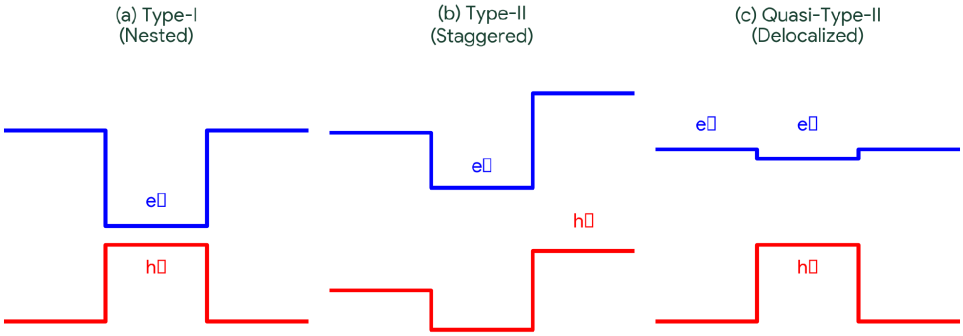

Figure 4: Energy band alignment diagrams tracking (a) nested Type-I, (b) staggered Type-II, and (c) delocalized Quasi-Type-II spatial electronic regimes inside heterostructure seeded nanorods.

5. Cutting-Edge Optoelectronic Circuitry and Memory Systems

Implementing bandgap-engineered quantum dots in solid-state devices has led to the development of new and sophisticated optoelectronic devices. These materials have been used to improve the performance of light-detection systems, especially in the deep-ultraviolet (DUV: 4.42 eV to 6.20 eV) spectral range. The conventional DUV photodetectors use the wide band gap bulk crystals which are fabricated by expensive and complex thin film vacuum deposition. The solution-processability and high quantum confinement provided by quantum dots can help in this regard, as they can extend the absorption threshold of moderately wide materials into the difficult DUV regime. For instance, quantum dots of ZnS with a size smaller than 10 nm increase the bandgap of materials to the high energy of DUV photons. The hybrid 0D/2D photodetectors with the use of ZnS QD inks deposited on p-type graphene/4H-SiC substrates exhibit remarkable spectral selectivity and response speeds, with a rise time

of 28 µs and decay time of 0.75 ms under continuous 250 nm DUV exposure. Also, ternary compositions such as CuInS2 or alloyed Cd1-xZnxS configurations are used in the multi-component layout of thin-film solar cells. These material choices enable the best wide-bandgap window layer device performance, with no forward current shunting microjunctions and traditional projector absorber thicknesses lowered to 150 nm by multiple light scatterings inside [6].

At the same time quantum dots have been used to develop optoelectronic non-volatile memory devices and neuromorphic hardware architectures that are inspired by biological synapses. Rapid photo-induced recovery under low intensity illumination at OFETs with floating gate of CdSe quantum dots makes them suitable for forming light-addressable memory states. The quantum dots in two-terminal all-inorganic capacitive memory devices (like spin-coated Al/ALPO/CdTe structures) act as localized charge storage nodes within a wide bandgap AlPO dielectric matrix within the memory device creating wide and reliable memory hysteresis curves for use as system-on-panel (SOP) display devices. Another use for halide perovskite quantum dots is as the active layer in arrays of resistors with random access memories (RRAMs, memristors) and in devices capable of encoding and storing information. Switching between high-resistance and low-resistance states, these memristive cells are switched by the application of an external electric field, with low operating voltages (~1 V) and high ON/OFF current ratios (more than 10^5).

This architectural structure featuring deposition of active QD layers within electronic junction structures is abstracted cross-sectionally in Fig. 5. The top contact metal electrode (Al, Au, etc.) and bottom conducting channel substrate (graphene, ITO or SiC matrices) are separated by the active layer made of tailored colloidal quantum dots. It is used as a structure for electrical switching in neuromorphic circuits, and for separating carriers by shortwave ultraviolet (UV) irradiation in solar-blind photodetectors [3][4][6].

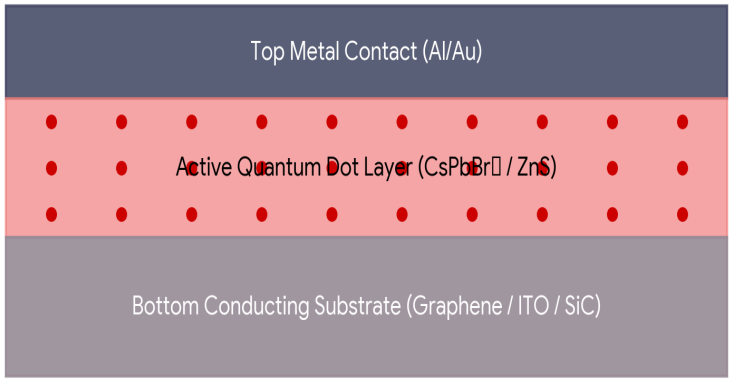

Figure 5: Cross-sectional schematic of an optoelectronic cell stack showing a colloidal quantum dot active layer embedded between top and bottom conducting contact lines.

6. Biomedical Theranostics: Bioconjugation, Biodistribution, and Toxicology

The unique optical characteristics of quantum dots such as broad continuous excitation spectrum, symmetrical and narrow emission spectrum, large Stokes shift and strong resistance to photobleaching, provide a number of advantages over conventional organic fluorophores like rhodamine 6G for biomedical bioimaging and diagnostics. The traditional organic dyes are very prone to fast and irreversible photo-bleaching in the clinic when exposed to light, and they have broad and asymmetric

emission peaks which interfere with multi-color tracking by spectral cross-talking. The ability of quantum dots to detect more than one color using a single wavelength of excitation light eliminates these drawbacks. Recently, near-infrared (NIR: 700 to 1400 nm) emitting quantum dots, including alloyed CdTe or InAs systems, have been studied for long-term tracking in living tissue. The NIR window offers a unique diagnostic benefit because it is in an optical window where there is minimal tissue autofluorescence and a high optical penetration depth, for deep-tissue tracking of tumour margins and targeted cancer treatment.

Translating the quantum dots from non-biological to biological solutions is challenging due to their natural hydrophobic properties, however.The challenge with translating the quantum dots from non-biological to biological solutions is that they are naturally hydrophobic, requiring robust surface modification to overcome the hydrophobicity. The quantum dots prepared by the classical pyrolytic organic methods are covered with hydrophobic ligands such as trioctylphosphine oxide (TOPO) or oleic acid and they immediately agglomerate and precipitate in water. To overcome this, two major surface engineering methods are applied: Amphiphilic Polymer Encapsulation and Ligand Exchange. The native hydrophobic ligands are preserved in Amphiphilic Polymer Encapsulation, in which the hydrophobic interactions allow the wrapping of the dots with amphiphilic polymer coating (for example, the maleic anhydride backbone or the phospholipids with PEG derivative). The photoluminescence quantum yields are kept close to those obtained prior the encapsulation. In contrast, Ligand Exchange removes the original organic molecules completely and attaches hydrophilic bifunctional linkers, such as mercatoundecanoic acid (MUA), dihydrolipoic acid (DHLA) or amino acids (L-histidine) directly to the nanocrystal surface. This results in a significantly reduced overall hydrodynamic diameter, but the direct surface coordination usually gives electronic defects, which lead to a 40% to 60% decrease in the emission quantum yield.

This is done by covalent attachment of biological molecules such as diagnostic peptides, aptamers, antibodies, or oligonucleotides to the water-solubilized dots to create site-specific target recognition. Traditional coupling uses amide bond chemistry to join carboxy-functional dots to amine-functional antibodies via carbodiimide (EDC/NHS) chemistry. Bioconjugated complexes of amine-functionalized IgG antibodies with core/shell CdSe/ZnS dots, for example, have a 100-fold higher sensitivity than assays of the same antibody conjugated with organic dyes for the detection of bacterial pathogens, such as Salmonella typhi, at low concentrations (100 cells/mL). The traditional EDC coupling, however, has a low coupling efficiency because of the fast hydrolysis of ester in water. To solve the above problem, modern research has shifted to the use of bio-orthogonal click chemistry, especially strain-promoted azide-alkyne cycloaddition (SPAAC) and norbornene-tetrazine click reactions. These click reactions are copper-free, proceed quickly at room temperature and achieve excellent reaction yield, and avoid the quenching effect of photoluminescence of copper ions on the reaction, allowing live virus labeling and real-time cellular imaging [6].

However, clinical translation is restricted by barriers of systemic biodistribution and the chronic heavy metal toxicity that currently exists. Injected intravenously, quantum dots act as foreign nanocolloids, and are immediately opsonized, presenting a distinct "protein corona" of serum proteins on the quantum dot surface. This marking encourages the uptake of particles into the reticuloendothelial and mononuclear phagocyte systems (RES/MPS) leading to high but non-specific uptake in liver, spleen, lymph nodes and bone marrow, with hardly any natural clearance. Particles must be engineered to be net neutral on their

surface to avoid macrophage recognition, to be sub-10nm in hydrodynamic diameter to be cleared by the kidneys and to have a high density of PEG brushes to prevent protein uptake. Importantly, when the inorganic surface coating on the surface starts to wear away, the core matrix can release very dangerous heavy-metal ions (free Cd2+ or Pb2+) into the intracellular environment. These free ions elicit oxidative stress through the formation of reactive oxygen species (ROS) which lead to DNA damage and organ failure. As a result, current efforts are directed toward the development of completely heavy metal free alternatives like biocompatible carbon quantum dots (CQDs), N doped carbon dots (NCQDs), and indium phosphide (InP) cores, which requires high optoelectronic performance in conjunction with good bio-safety in long-term use [3][4][7].

7. Conclusion and Future Perspectives

The collection of these seven research tracks indicates the strong maturity of the development of semiconductor quantum dots from the fundamental science models to complex architectures. Incorporating new mirror-type boundary conditions further stresses the need for solid-state theory to be in tune with experimental realities. At the same time, multi-component architectural engineering illustrated by seeded nanorods elucidates the advantages of combining geometric shapes to improve multi-photon absorption and guide charge-carrier trajectories. But, if commercialization is to take place, there must be clear solutions to the current trade-offs. Achieving higher optoelectronic efficiencies of the heavy-metal core materials is still hampered by high toxicity and strict environmental regulations, and the greener materials based on carbon or silicon still have low emission quantum yields and wider emission spectra. Advanced future developments will be enabled by a closer coupling of machine-learning enabled chemical syntheses, the development of architectures that are stable and do not use heavy metals and advanced bio-orthogonal surface functionalizations. Addressing these challenges will further enhance the potential quantum dots have for clinical medicine and optoelectronic hardware.

References

1. H. I. Ikeri, A. I. Onyia, and V. M. Adokor, “Theoretical model for Bandgap Engineering of Semiconductor Quantum Dots,” *J. Phys. Chem. Mater.*, vol. 8, no. 3, pp. 34–40, Sep. 2021, doi: 10.26438/ijpcas/v8i3.3440.
2. T. Torchynska and Y. Vorobiev, “Semiconductor II-VI Quantum Dots with Interface States and Their Biomedical Applications,” in *Advanced Biomedical Engineering*, Dr. Gaetano Gargiulo, Ed. Rijeka, Croatia: InTech, 2011, pp. 143–178, doi: 10.5772/20314.
3. M. Afzaal and P. O’Brien, “Recent developments in II-VI and III-VI semiconductors and their applications in solar cells,” *J. Mater. Chem.*, vol. 16, no. 16, pp. 1597–1602, Apr. 2006, doi: 10.1039/B512182E.
4. A. Sitt, I. Hadar, and U. Banin, “Band-gap engineering, optoelectronic properties and applications of colloidal heterostructured semiconductor nanorods,” *Nano Today*, vol. 8, no. 5, pp. 494–513, Oct. 2013, doi: 10.1016/j.nantod.2013.08.002.
5. H. K. Lee, T. Park, and H. Yoo, “Device Applications Enabled by Bandgap Engineering Through Quantum Dot Tuning: A Review,” *Materials*, vol. 17, no. 21, p. 5335, Oct. 2024, doi: 10.3390/ma17215335.
6. A. M. Wagner, J. M. Knipe, G. Orive, and N. A. Peppas, “Quantum Dots in Biomedical Applications,” *Acta Biomater.*, vol. 94, pp. 44–63, Aug. 2019, doi: 10.1016/j.actbio.2019.05.022.
7. K. Agarwal, H. Rai, and S. Mondal, “Quantum dots: an overview of synthesis, properties, and applications,” *Mater. Res. Express*, vol. 10, no. 6, p. 062001, Jun. 2023, doi: 10.1088/2053-1591/acda17.